

Visible Light Photocatalytic Degradation of Azo Dye and a Real Textile Wastewater Using Mn, Mo, La/TiO₂/AC Nanocomposite



S. Jorfi,^{a,b} S. Mirali,^b A. Mostoufi,^c and M. Ahmadi^{a,b,*}

^aEnvironmental Technologies Research Center, Ahvaz Jundishapur University of Medical Sciences, Ahvaz, Iran

^bDepartment of Environmental Health Engineering, Ahvaz Jundishapur University of Medical Sciences, Ahvaz, Iran

^cDepartment of Medicinal Chemistry, Ahvaz Jundishapur University of Medical Sciences, Ahvaz, Iran

doi: 10.15255/CABEQ.2017.1261

Original scientific paper
Received: October 25, 2017
Accepted: May 18, 2018

Mn, Mo, La/TiO₂/activated carbon (AC) photocatalysts were synthesized by sol-gel method. The prepared samples were characterized by XRD, FT-IR, BET, DRS, and FE-SEM techniques. The findings revealed that the synthesized catalysts were anatase type and nano-sized particles. The catalysts exhibited high adsorption ability in the visible light region with a red shift in the adsorption edge. The formation of Mn, Mo, La/TiO₂/AC crystallites in the activated carbon was confirmed by FE-SEM. The effects of initial dye concentration, catalyst dosage, reaction time, and solution pH were investigated for removal of Reactive Red 198. According to the obtained results, the maximum removal efficiency of 91 % was obtained at initial dye concentration of 20 mg L⁻¹, pH of 3, and catalyst concentration of 2 g L⁻¹. Synthesized nano-photocatalyst showed reasonable photo degradation efficiency of 84 % for initial COD concentration of 4700 mg L⁻¹ in treatment of a real textile wastewater sample. GC/MS analysis of raw and treated wastewater confirmed degradation and producing of simple intermediates during the photocatalytic process.

Key words:

advanced oxidation technology, Mn, Mo, La/TiO₂/activated carbon nanocomposite, photocatalytic degradation, Azo dye, textile wastewater

Introduction

Dyes are the most important existing pollutants in textile wastewaters. These compounds are often toxic, carcinogenic, and mutagenic to living organisms, chemically and photo-chemically stable, and non-biodegradable^{1,2}. Based on the literature, a large number of dye molecules has been categorized as carcinogenic substances. Reactive red 198 is one of the azo dyes that is currently used in textile industries³. As conventional processes are not efficient for degradation of recalcitrant compounds in water and wastewater, nowadays, advanced oxidation processes (AOPs) are utilized for degradation and mineralization of emerging pollutants, and are based on generation of free radicals with high reactivity^{4,5,6}. Among AOPs, noticeable attention has been paid to photocatalytic degradation of organic compounds by semiconductors. In recent years, significant progress in scientific technologies has made acutely high demands on semiconductor materials⁷. A set of

semiconductors, including oxides, sulfides, etc., has been increasingly used as photocatalysts⁸. Among these semiconductors, nano-sized TiO₂ has received much attention, because of its wide applications in semiconductors, sensors, antibacterial and hygienic materials, photocatalysts, and solar cells⁹. TiO₂ exhibits high photocatalytic activities, high turnover, long-term photostability, cost-effectiveness, and non-toxic nature¹⁰⁻¹³. Therefore, it has been extensively used in various photocatalytic fields, such as water and gas streams purification and degradation of organic pollutants. Photocatalytic degradation offers great potential as an advanced technology to detoxify pollutants^{14,15,16}.

Usually, titanium dioxide can exist as three crystalline polymorphs, namely, anatase (tetragonal), brookite (orthorhombic), and rutile (tetragonal)^{17,18,19}. However, they have shown various photocatalytic activities, due to variations in their physical and crystallographic properties^{20,21}. Anatase is the most photoactive phase of TiO₂, due to its particular crystallographic structure, which increases electron-hole recombination times^{22,23}.

*Corresponding author: ahmadi241@gmail.com

An important drawback of photocatalytic activities of TiO_2 is a wide band gap (3.2 eV for anatase) that requires UV light during the photocatalytic reaction, or, in other words, only a small fraction of solar energy, about 4–5 %, is adsorbed, which leads to inefficient photocatalytic reaction when using sunlight^{24–27}. The problem of the high recombination rate of electron-hole pairs is charging the carriers separation, leading to their inability to be useful²⁸. Consequently, researchers have studied the modification of the structure/composition for effective utilization of the solar spectrum, the visible light region and the photocatalytic performance²⁶. Therefore, in recent years, many methods have been applied to improve the energy band gap and increase the light adsorption by TiO_2 . The modification approaches, such as reduction in particle size, increasing the surface area, doping and loading, all aimed to replace the adsorption of UV by visible light and increase the life-time of electron-hole pairs²⁵. Previous studies have shown that doping with metals improved the photocatalytic efficiency of TiO_2 , and could be considered as a promising strategy²⁵. The verified metal dopants, including Mn^{30,31}, Cu, Co³², Ag³³, La³⁴, Sn³⁵, and so on, not only reduced the rate of recombination of electron/hole, but also increased the adsorption in the visible light region²⁷. Extensive studies have been carried out in terms of mono doping TiO_2 with transition metals, such as La, Ag, Mn, Co, Cu, Mo, Au, Pt, etc³⁴. It has been reported that TiO_2 doped with two or three elements significantly improved the adsorption of light in the visible light range and increased the photocatalytic activities³⁶. For instance, Li *et al.*²⁷ reported that Mo-Sb-S tridoped TiO_2 nanoparticles exhibited outstandingly enhanced visible light driven for degradation of methylene blue. Elsellami *et al.*²³ used sol-gel method to manufacture visible active Li-Cd-La tridoped TiO_2 photocatalyst. Hua *et al.*⁸ confirmed that W-La codoped TiO_2 nanomaterials improved the photocatalytic activities more than a single-doped W/ TiO_2 system, providing an obvious decrease in band gap energy. Quan *et al.*³⁰ prepared Mn-N codoped TiO_2 photocatalyst with improved halogen lamp which induced photocatalytic activity. Akbarzadeh and Javadpour³⁷ synthesized W/Mo codoped TiO_2 photocatalyst for enhancement of Methylene Blue removal under sunlight. Liu *et al.*³⁸ reported that Mo-N/ TiO_2 photocatalyst, which was synthesized by sol-gel method, had higher activity than undoped and Mo- or N-doped TiO_2 catalyst.

Separation and recovery of nanoparticles from reaction solution is difficult during application of TiO_2 nanoparticles³⁹. To tackle this problem, loading TiO_2 nanoparticles on some supporting materials has been proposed⁴⁰. Among the various supporting materials, activated carbon is an attractive

candidate, due to its porous structure, significant adsorption capability, hydrophobic and hydrophilic properties, eco-friendly nature, structural stability, mechanical resistance, high surface area, and cost-effectiveness⁴¹. This was the first time that Mn, Mo, La/ TiO_2 nanoparticles supported on activated carbon were used for degradation of Reactive Red 198 (RR 198) under visible light irradiation, and also the first time that the decolorization and degradation performance was evaluated for real textile wastewater; moreover, the intermediate compounds that had formed during the photocatalytic process were identified.

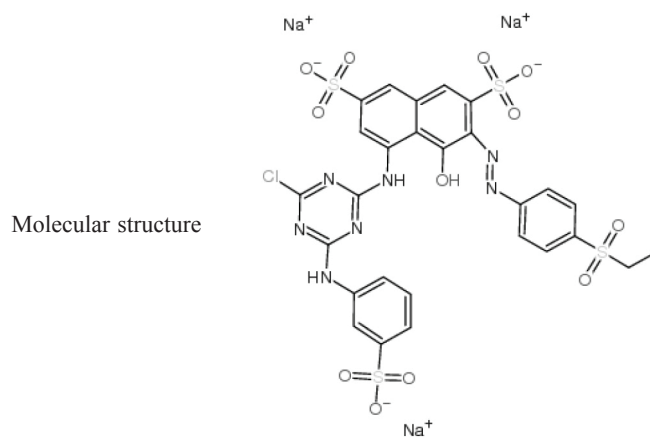
Materials and methods

Materials

Reactive Red 198 (RR 198) used to determine the performance of the catalyst was bought from Alvan Sabet Co. Hamadan, Iran. Chemical and physical properties are shown in Table 1. Ethanol ($\text{C}_2\text{H}_6\text{O}$), sulfuric acid (95–97 %), nitric acid (65 %), hydrochloric acid (98 %), titanium tetraisopropoxide ($\text{C}_{12}\text{H}_{28}\text{O}_4\text{Ti}$), lanthanum nitrate hexahydrate ($\text{La}(\text{NO}_3)_3 \cdot 6\text{H}_2\text{O}$), ammonium heptamolybdate tetrahydrate ($(\text{NH}_4)_6\text{Mo}_7\text{O}_{24} \cdot 4\text{H}_2\text{O}$), and manganese (II) sulfate monohydrate ($\text{MnSO}_4 \cdot \text{H}_2\text{O}$), sodium hydroxide (NaOH), 2-propanol ($\text{C}_3\text{H}_8\text{O}$) were all analytical grade and obtained from Merck Co., Germany. Deionized water was used for preparation of all solutions/suspensions.

Table 1 – Properties of RR 198 dye

Parameter	Characteristics
Chemical formula	$\text{C}_{27}\text{H}_{18}\text{ClN}_7\text{Na}_4\text{O}_{15}\text{S}_5$
Class	Azo
C.I. number	18221
Molecular weight (g mol^{-1})	967.5
λ_{max} (nm)	518



Preparation of photocatalysts

Mn, Mo, La/TiO₂/AC was prepared by sol-gel method using titanium tetraisopropoxide (TTIP), lanthanum nitrate hexahydrate (La(NO₃)₃·6H₂O), ammonium heptamolybdate tetrahydrate (NH₄)₆Mo₇O₂₄·4H₂O, and manganese(II) sulfate monohydrate (MnSO₄·H₂O) as titanium, lanthanum, molybdenum, and manganese sources, respectively^{28,42}. A homogeneous solution of TTPP (0.5 M) in 2-propanol (85 mL) was prepared under vigorous stirring during 1 h. Nitric acid was used to adjust the solution pH and for suppressing the hydrolysis process of the solution. The solution was vigorously stirred for 1 h in order to form sols, and subsequently sonicated for 15 min (solution A).

Doping of TiO₂ with Mo, Mn, and La was carried out by adding solution containing known concentrations of 0.25 to 0.5 % (w/v) of ammonium heptamolybdate tetrahydrate, manganese (II) sulfate monohydrate, and lanthanum nitrate hexahydrate, respectively, (in 1:1 (v/v) of water and 2-propanol) dropwise with stirring to solution A (solution B).

After stirring solution B for 15 h, the formed gelatinous material (tridoped TiO₂) was sonicated for 15 min, centrifuged (for 15 min, 3000 rpm), and washed with deionized water. A certain amount of activated carbon was added to solution B, followed by sonication in an oven at 100 °C for 3 h to perform aging phase. The obtained powder was manually ground and calcinated at 450 °C for 4 h. In this study, based on various percentages of elements, eight nano-photocatalysts were prepared, and the concentrations of elements in each sample are shown in Table 2.

Preparation of activated carbon

Firstly, 5 g of granulated activated carbon was mixed with 50 mL of deionized water, followed by boiling for 15 min at 100 °C. Thereafter, the suspension was cooled down to room temperature, filtered, and dried for 3 h at 105 °C.

Table 2 – Dye removal efficiency in eight different synthesized nanocomposites with different proportions of Mo, Mn and La, RR 198 60 mg L⁻¹, irradiation time: 60 min, pH: 7, photocatalyst: 2 g L⁻¹

Elements	Sample code							
	1	2	3	4	5	6	7	8
Mn (%)	0.50	0.25	0.50	0.50	0.25	0.25	0.50	0.25
La (%)	0.50	0.25	0.50	0.50	0.50	0.25	0.25	0.50
Mo (%)	0.50	0.25	0.25	0.50	0.25	0.50	0.25	0.50
Activated carbon (g)	0.250	0.125	0.208	0.208	0.165	0.165	0.165	0.208
Removal (%)	28.56	26.45	82.04	16.45	84.17	6.50	44.38	51.73

Characterization techniques

X-ray diffraction (XRD) patterns of all samples were characterized in the range of 10–80° (2θ) using an X-ray diffractometer (Philips, PW, 1840; Netherlands) with Cu Kα radiation (λ = 0.15418 nm). The accelerating voltage and the applied current were 40 kV and 30 mA, respectively. The average crystallite size was calculated by Debye Scherer formula (Eq. (1)):

$$D = \frac{K\lambda}{\beta \cos \theta} \quad (1)$$

where, D is crystallite size (nm), K is share factor (0.89), λ is wavelength (0.15418 nm), θ is diffraction angle, and β is full width at half maximum (FWHM)¹⁰.

Specific surface areas were determined using BET analysis (Nano SORD 92, Iran). Fourier-transform infrared spectra (FTIR) of the samples were prepared (Bruker, Model: VERTEX70, Germany) between the frequency ranges of 400–4000 cm⁻¹ with KBr as a diluent¹⁰. The diffuse reflectance spectra (DRS) were obtained using a UV-visible spectrophotometer (JASCO, V-670- Japan)⁴³. The surface characteristics and morphological features of nanocomposite and also elemental composition were studied using a field emission scanning electron microscope (FE-SEM, TESCAN microscope equipped with energy dispersive X-ray (EDX) microanalysis, Mira3, Kohoutovice, Czech Republic)⁴⁴.

Photocatalytic degradation

Photocatalytic degradation of RR 198 was studied through calculation of RR 198 removal in aqueous solution. A glass reactor was used and a visible light Xenon lamp (50 W, 110 Lux) was applied for performing irradiation. The distance between Xenon lamp and RR 198 solution container was 10 cm. The reactor was filled with 200 mL of dye solution of defined concentration, and 2 g L⁻¹ of a selected photocatalyst. Afterwards, solution was stirred for 15 min in the dark to establish the adsorption equilibrium. Samples were collected at specific times during irradiation, followed by centrifuging prior to use. The residual concentration of RR 198 was measured using a UV-Vis spectrophotometer (DR-5000) at λ_{max} of 518 nm, and the degradation efficiency was calculated by Eq. (2)

$$\text{Degradation efficiency (\%)} = \frac{(C_0 - C_t)}{C_0} \cdot 100 \quad (2)$$

where, C_0 and C_t are the initial and the residual RR 198 concentrations (mg L⁻¹), respectively.

The maximum decoloration rate at the same conditions was considered as a best criterion for selecting the desired photocatalyst among the different samples investigated. RR 198 degradation experiments were carried at defined conditions (initial dye concentration: 60 mg L⁻¹, catalyst dosage: 2 g L⁻¹, pH: 7± 0.3, contact time: 1 h, and irradiation: visible light). Using the selected photocatalyst, the effect of operating parameters was studied and the photo-degradation experiments on a real textile wastewater were performed.

Real textile wastewater degradation

A set of experiments was conducted on a real textile wastewater, obtained from a local industry, based on optimum conditions found in previous stages. Qualitative analysis of raw and treated wastewater was carried out by gas chromatography–mass spectrometry (GC-MS) analysis (Model: Agilent 7890, USA) with HP-5MS capillary column (30 m × 0.25 mm × 0.25 μm film thickness, 5 % phenyl – 95 % methyl siloxane phase). The carrier gas (Helium) was fed into the system at a 1 mL min⁻¹ stable flow rate. Firstly, the oven temperature rate was adjusted to 40 °C for 1 min, followed by an increase to 300 °C at 5 °C min⁻¹, which was kept constant for around 3 min. Ultimately, the sample was injected into the instrument at a splitting ratio of 10:1.

Results and discussion

Selection of photocatalyst

Following the fabrication of eight nanocomposite samples, photo-degradation process was performed to select the best proportion of metals in synthesized nanocomposites. As shown in Table 2, sample No. 5 with removal efficiency of 84.17 % showed the best performance in dye removal, and this sample was selected for the remaining experiment and characterization.

Characterization of Mn, Mo, La/TiO₂/AC nanocomposite

Fig. 1 shows XRD patterns of the prepared Mn, Mo, La/TiO₂/AC nanocomposite. The main dominant peaks of pure TiO₂ were found at 2θ of 25.5, 38, 48, 53, and 55°, which are in good agreement with the standard Joint Committee on Powder Diffraction Standards (JCPDS) card No: 21 – 1272, and are often taken as the characteristic peaks of anatase phase. There was no rutile diffraction peak in XRD pattern of Mn, Mo, La/TiO₂/AC nanocomposite. The peaks appearing at 2θ of 26, 37, 41.8, 49.8, 60.3, 63, 66, 69, 72, and 79° belonged to Mo (JCPDS: 01-0615). Similar results are reported in the literature⁴⁵. The average crystallite size of Mn, Mo, La/TiO₂/AC nanocomposite was found to be about 8.15 nm, according to Scherer's equation.

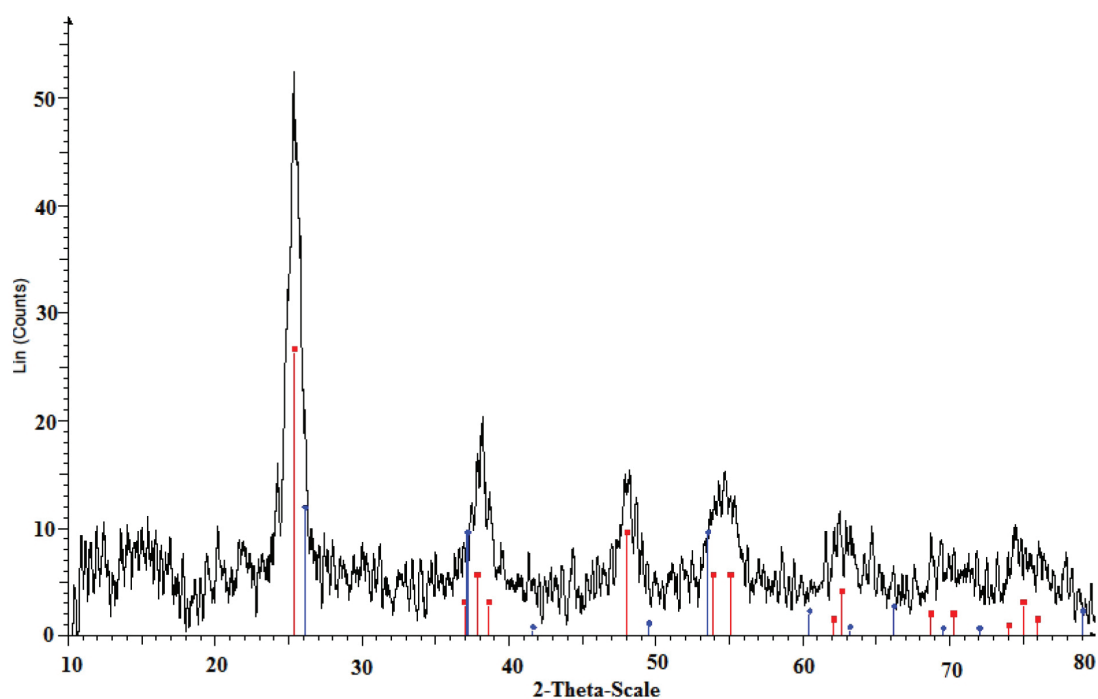


Fig. 1 – XRD pattern of Mn, Mo, La/TiO₂/AC catalyst

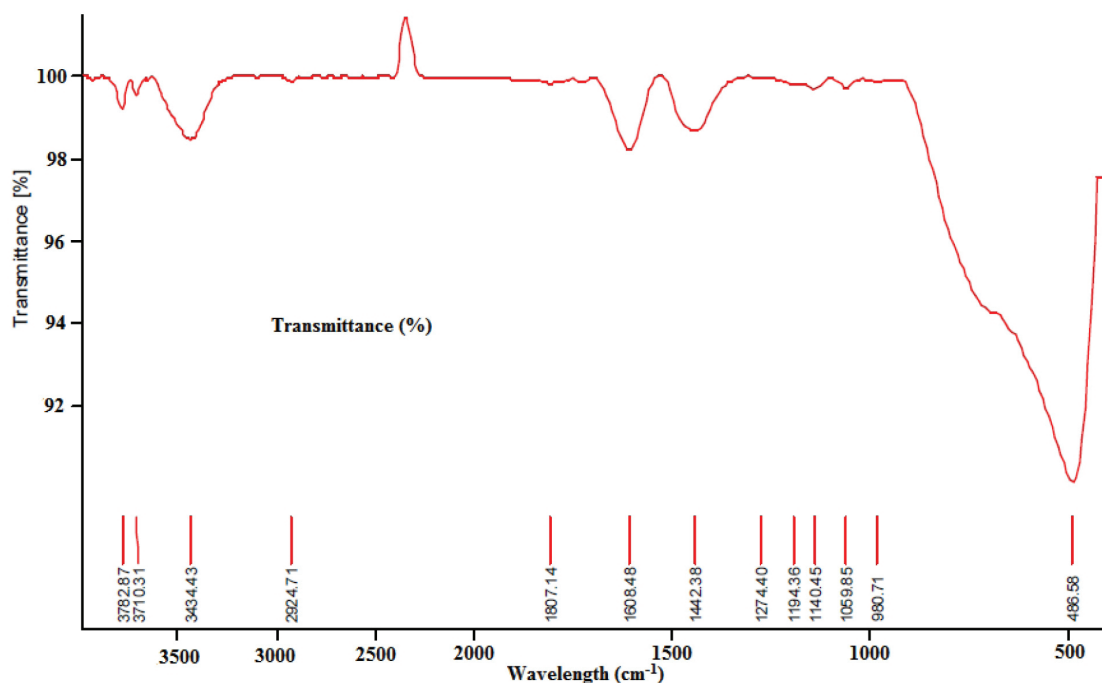


Fig. 2 – FT-IR spectrum of Mn, Mo, La/TiO₂/AC nanocomposite

BET analysis showed that the specific surface area of nanocomposite was 97.525 m² g⁻¹, while the specific surface area of activated carbon before loading with doped TiO₂ was 973.65 m² g⁻¹. This confirmed that TiO₂ and doped elements had occupied a large surface area of activated carbon.

FT-IR spectrum of Mn, Mo, La/TiO₂/AC nanocomposite was prepared in the range of 500 to 4000 cm⁻¹, and is shown in Fig. 2. The catalyst spectrum showed four peaks at 486.58, 1442.38, 1608.48, and 3434.43 cm⁻¹. The absorption bands of 3100–3700 cm⁻¹ and 1600–1640 cm⁻¹ were assigned to the stretching vibration and bending vibration, respectively, of the hydroxyl groups present on the surface of TiO₂ catalyst⁴⁵. Peaks in the regions of 3434.43 cm⁻¹ and 1608.48 cm⁻¹ were respectively related to the bond stretching and bending –OH groups caused by the adsorbed water molecules and hydroxyl groups. These groups are critical in the photocatalytic degradation of dye molecules. The peak appearing at 1442.38 cm⁻¹ was related to –CH and carboxyl group, due to adsorption of carbon dioxide. The wide peak in the region of 486.58 cm⁻¹ was related to the bend vibration of Ti-O-Ti and Ti-O bonds⁴⁴. Additionally, the absorption band around 2924.71 cm⁻¹ was assigned to the stretching vibration of C-H¹³. FT-IR spectra of the sample showed no band characteristic of metal oxides. It could be due to low metal concentrations, and thus low intensity of bands, as well as overlapping of bands associated with flexural vibrations of Ti-O bond⁴⁶ flexural vibrations (in the area 500–1000 cm⁻¹) and characteristic La-O, Mn-O, Mo-O bands.

UV-Vis diffuse reflectance spectra (DRS) of Mn, Mo, La/TiO₂/AC, Mn, Mo, La/TiO₂, Mn, La/TiO₂, La/TiO₂, Mn, La/TiO₂, Mo, La/TiO₂ and pure TiO₂ catalysts were analyzed (Fig. 3). It is obvious that pure TiO₂ showed absorption band in the UV area, while the other samples had shifted to the visible light spectra (400 – 510 nm)⁴⁴. This shift in the adsorption edge reduced the direct band gap of doped activated carbon catalysts, compared to pure TiO₂, due to incorporating Mn, Mo, and La into the TiO₂ network and stabilizing doped TiO₂ on activated carbon⁴⁵. The band gap energy can be approximately calculated using Eq. (3):

$$E = \frac{hc}{\lambda} \quad (3)$$

where, h is Planck constant (4.135×10^{-15} eV), E is band gap energy (eV), c is speed of light ($3 \cdot 10^8$ m s⁻¹), and λ is wavelength (nm). In Table 3, the band gap energy of studied samples was calculated⁴⁷. According to Fig. 3 and the reported energy band gap in the Table 3, the red shift in the DRS spectrum increases and band gap energy shows a decrease with an increase in the content of doped elements in TiO₂ network, which improves light adsorption and optical activity of TiO₂ catalysts⁴⁵.

The morphology and size distribution of Mn, Mo, La/TiO₂/AC nanocomposite were investigated by FE-SEM (Fig. 4a). According to the microscopic structure of catalyst, particle size was in the range of 7–11 nm. Black holes in the image were probably related to activated carbon particles, which were found to be non-uniformly distributed within the catalyst network.

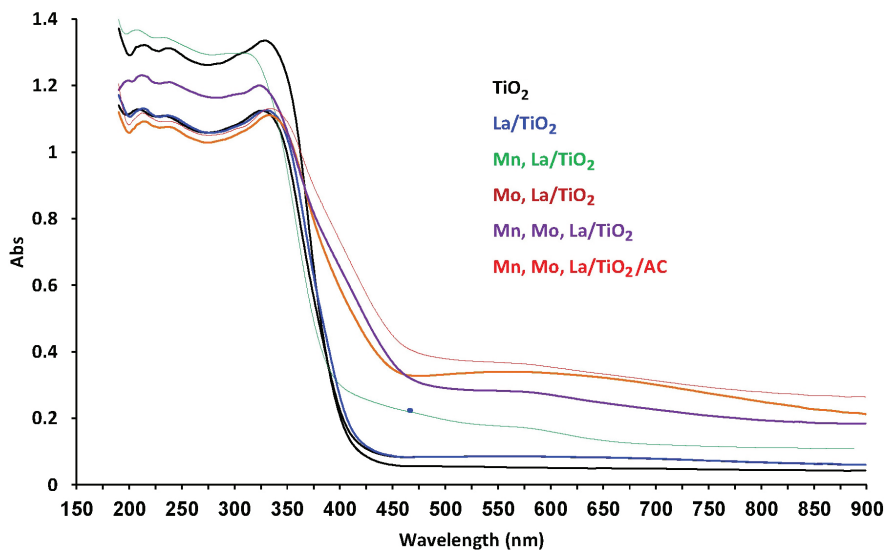


Fig. 3 – UV-vis diffusion reflectance spectra of pure TiO_2 and fabricated catalysts

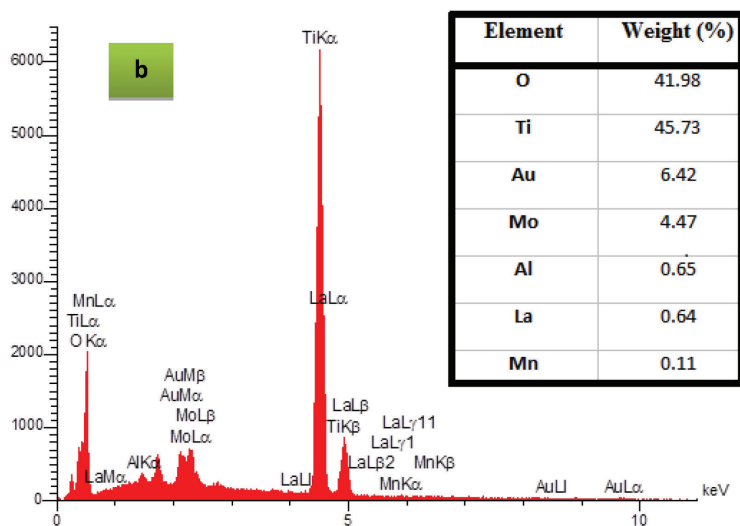
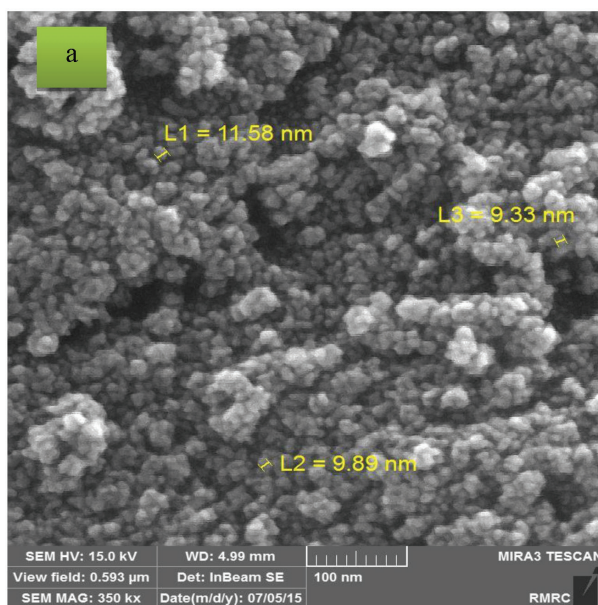


Fig. 4 – FE-SEM (a) and EDS (b) of $\text{Mn, Mo, La/TiO}_2/\text{AC}$ nanocomposite

Table 3 – Wavelength and band gap energy of fabricated TiO_2 catalysts

Catalyst	Wavelength (nm)	Band gap energy (eV)
TiO_2	399	3.10
La/TiO_2	416	2.98
Mn, La/TiO_2	425	2.91
Mo, La/TiO_2	523	2.37
Mn, Mo, La/TiO_2	545	2.27
$\text{Mn, Mo, La/TiO}_2/\text{AC}$	552	2.24

Qualitative elemental analysis, using EDS technique (Fig. 4b), confirmed the presence of Mn, Mo, La, and AC¹⁸. Based on the EDS analysis, synthesized nanocomposite contained 0.25 % Mo, 0.5 % La, 0.25 % Mn, and 0.165 % carbon. Results confirmed the desired purity of synthesized nanocomposite.

Photocatalytic degradation of Reactive Red 198

Effect of pH

Any changes in pH of aqueous solution simultaneously alter the surface features of adsorbent and structure of the adsorbate molecules. Hence, the study of photocatalytic removal of a typical contaminant affected by solution pH is of great importance. Effect of solution pH on photocatalytic performance was evaluated in the range of 2–9. The photocatalytic degradation of pollutant was significantly influenced by solution pH where the highest removal was obtained at lower pH values. Results showed that the degradation performance enhanced from 36.9 to 78.7 % along with decreasing solution pH from 9 to 2 during 60 min reaction. The initial pH value of 3 with corresponding removal of 78.3 % was selected as an optimum point for photo-degradation reaction. Alkaline pH value of 9 adversely affected the photocatalytic degradation and the removal declined to 36.9 % (Fig. 5). Regarding the lack of a significant difference between dye removal efficiencies at pH 2 and 3, and also the ease of operation, initial pH 3 was selected as an optimum solution pH for the following experiments.

The pH_{zpc} of nanocomposite was determined to be 6.3. Therefore, it is obvious that, at pH values of 6.3 and above, the surface charge of synthesized composite is positive. Considering the pH_{zpc} of nanocomposite, higher tendency of RR 198 adsorption onto the surface of nanocomposite was observed at pH values less than 6.3. Therefore, a significant improvement would occur in photocatalytic removal of dye molecules. By increasing pH of aqueous solution, an enhancement was observed in

the number of attachment sites with negative charges. This phenomenon leads to decreasing the adsorptive removal of dye molecules by the nanocomposite, because of the role of electrostatic repulsive forces. Furthermore, another factor that leads to decreasing dye removal efficiency at higher pH values is the excessive number of hydroxyl ions competing with dye molecules to occupy the surface reactive sites of adsorbent.

Effect of nanocomposite dosage

The influence of Mn, Mo, $\text{La/TiO}_2/\text{AC}$ nanocomposite dosage (1–6 g L^{-1}) on the photocatalytic degradation of Azo dye RR 198 was studied at pH 3, dye concentration of 60 mg L^{-1} and during 60 min contact time. Based on the findings, by increasing the amount of catalyst to 5 g L^{-1} , an improvement was seen in RR 198 removal. However, further increase in the quantity of catalyst had not significantly changed the removal rate of RR 198. The removal efficiencies for photocatalyst dosages of 1, 2, 3, 4, and 5 g L^{-1} were 55.29, 78.73, 80.3, 82.27, and 83.3 %, respectively (Fig. 6). Increasing

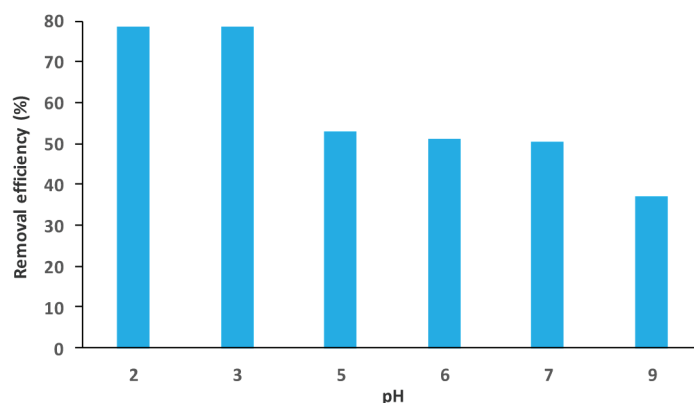


Fig. 5 – Effect of pH on Azo dye degradation by Mn, Mo, $\text{La/TiO}_2/\text{AC}$ nanocomposite under visible light irradiation (catalyst dosage 2 g L^{-1} , RR 198: 60 mg L^{-1} , irradiation: visible light)

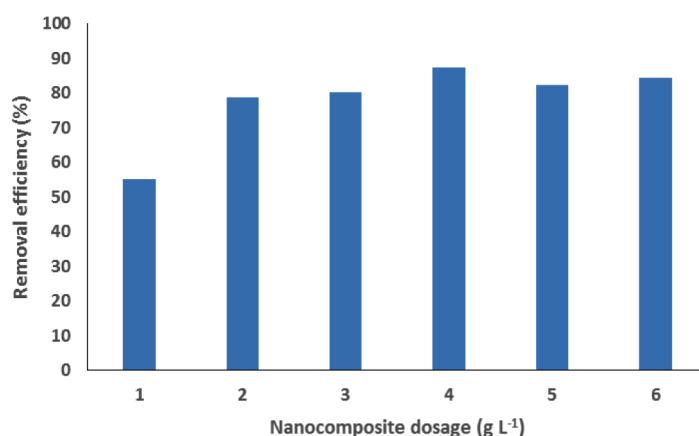


Fig. 6 – Effect of Mn, Mo, $\text{La/TiO}_2/\text{AC}$ nanocomposite dosage on RR 198 photo-degradation (pH: 3, RR 198: 60 mg L^{-1} , irradiation: visible light)

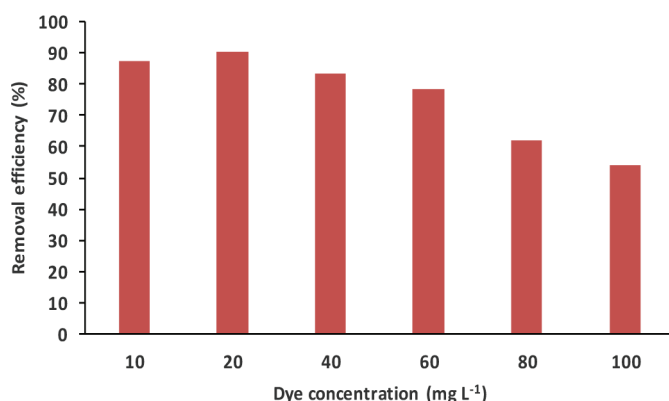


Fig. 7 – Effect of RR 198 concentration on photo-degradation reaction (pH = 3, catalyst dosage = 2 g L⁻¹, irradiation: visible light)

the removal rate of dye with an enhancement in the quantity of catalyst can be attributed to increasing the amount of surface area that creates a higher number of reactive sites for the photocatalytic reaction and adsorption of visible light by photocatalyst. This increase in surface area provides higher amounts of OH[•] that act in favor of photocatalytic removal of contaminant molecules.

However, as shown in Fig. 6, the removal rate of dye molecules had no significant improvement over 5 g L⁻¹ photocatalyst dosages and remained relatively constant at 6 g L⁻¹ dosage. Further increase in the amount of photocatalyst above the optimum level caused the agglomeration of photocatalyst particles in aqueous media, which weakened the performance of surface reactive sites responsible for generating OH[•]. Since the lower catalyst usage is an advantage and there was no significant difference in removal efficiencies between photocatalyst dosages of 2 and 3 g L⁻¹, the photocatalyst dosage of 2 g L⁻¹ was selected for the remaining experiments.

Effect of initial RR 198 concentration

Effect of varying initial RR 198 concentrations in the range of 10–100 mg L⁻¹ on photocatalytic degradation process was studied at pH 3 (Fig. 7), photocatalyst dosage of 2 g L⁻¹ and visible light irradiation. Results indicated that the photo-degradation efficiency was reduced with increasing initial dye concentration, which is consistent with previous studies^{42,48}. Increased dye concentration adversely affects the efficiency of photo-degradation reaction through reduction of visible light penetration, occupation of nanocomposite active sites, as well as reduction in the interplay of photons with active sites⁴⁹.

Mineralization of RR 198

Mineralization of RR 198 through photo-degradation reaction was calculated using Eq. (4) and

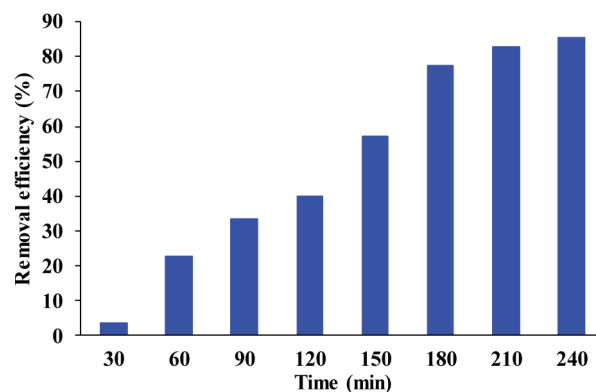


Fig. 8 – Mineralization of RR 198 azo dye using Mn, Mo, La/TiO₂/AC under visible irradiation (pH: 3, photocatalyst dosage: 2 g L⁻¹, initial RR 198 concentration: 60 mg L⁻¹)

COD analysis for the initial dye concentration of 60 mg L⁻¹, pH 3, photocatalyst dosage of 2 g L⁻¹ and reaction time of 240 min. After 120 min reaction, all dye molecules were decolorized. However, the high COD removal of 85 % (COD₀: 420 mg L⁻¹) was only achieved after 240 min (Fig. 8). The longer time required for COD removal, compared to decolorization, could be attributed to decomposition of RR 198 into intermediate metabolites, such as acetamide, methoxy-phenyl benzoic acid, and dodecanoic acid.

$$\text{Mineralization (\%)} = \frac{\text{COD}_0 - \text{COD}_t}{\text{COD}_0} \cdot 100 \quad (4)$$

where, COD₀ and COD_t are COD concentrations at beginning of the reaction and at time *t*.

Reusability test

Recovery of synthesized photocatalyst was investigated in five consecutive experimental runs at the same operating conditions (initial RR 198 concentration = 6 mg L⁻¹, photocatalyst dosage = 2 g L⁻¹, solution pH = 3, and reaction time = 60 min). Chemical regeneration of applied photocatalyst was carried out after each experimental run using 0.1 M H₂SO₄ solution within 45 min. Results indicated the acceptable stability and regeneration potential of synthesized photocatalyst. The degradation rates (%) of dye molecules from the first to the fourth run of experiments were as follows: 78.57, 72.4, 66.32, and 52.78 %, respectively (Fig. 9). The decrease in RR 198 removal efficiency after four consecutive runs was 25.79 %. Protonation of the photocatalyst surface during chemical regeneration, which leads to a decrease in dye adsorption rate, is probably the main reason for decreasing photocatalyst performance. Furthermore, consecutive regeneration would lead to the loss of photocatalyst from the activated carbon support, as well as the fouling of the photocatalyst surface by the intermediates of azo dye degradation.

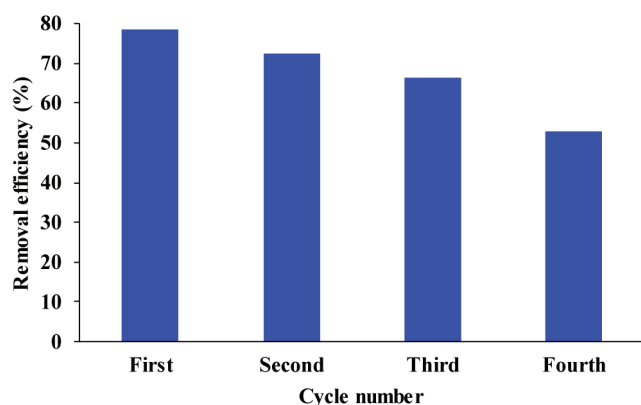


Fig. 9 – Reusability of Mn, Mo, La/TiO₂/AC nanocomposite within four consecutive cycles

Photo-degradation of a real textile wastewater

In order to investigate the capability of photo-degradation process using Mn, Mo, La/TiO₂/AC as a photocatalyst under visible irradiation, a set of experiments was conducted on a real textile wastewater containing various recalcitrant organics and color compounds. The average concentrations of COD and BOD₅ of raw textile wastewater were 4700 and 510 mg L⁻¹, respectively (Table 4). This wastewater was characterized as a recalcitrant wastewater, due to low BOD₅/COD ratio of 0.1, indicating the presence of non-biodegradable compounds and the necessity for applying advanced oxidation options. The qualitative investigation of raw wastewater contents was performed via GC/MS analysis (Table 5), which showed that the principal identified organics of raw wastewater included quinolone, fluoroacetamide, dimethylquinoline, methylquinoline, methylisoquinoline, linoleic acid, tri-butyl phosphate and palmitic acid.

The average COD concentration of raw textile wastewater was 4700 mg L⁻¹ which decreased to 740 mg L⁻¹ in the effluent of photocatalytic process using Mn, Mo, La/TiO₂/AC nanocomposite after 6 h, corresponding to COD and TOC removal rates of 84 and 81 %, respectively (Table 6).

Advanced oxidation processes are characterized by rapid partial oxidation and long-term mineralization. The experimental conditions were set as determined for synthetic wastewater with RR 198 azo dye (solution pH = 3, catalyst dosage = 2 g L⁻¹, reaction time = 300 min). The residual COD concentration of raw textile wastewater was 740 mg L⁻¹ after 300 min, corresponding to COD removal of 84 %. The possible reasons for the low removal rate in comparison with synthetic wastewater would be the insufficient light energy and photocatalyst for degradation of recalcitrant organic molecules, as well as the lack of UV capability of penetration in aque-

Table 4 – Characteristics of raw wastewater

Parameter	Value	
	Range	Average
COD (mg L ⁻¹)	3720–5815	4700
BOD ₅ (mg L ⁻¹)	465–570	510
BOD ₅ /COD	–	0.1
TOC (mg L ⁻¹)	2580–3490	2940
TDS (mg L ⁻¹)	12040–14600	13280
pH	7.2–8.1	7.8
Turbidity (NTU)	15–30	24

ous media, due to high turbidity. According to Table 7, the intermediate metabolites of treated textile wastewater were as follows: acetamide, dimethyl propane, isoindole, bromoform, methoxy phenyl benzoic acid, cycloheptatriene, benzaldehyde, acetate esters, benzoxazine, benzothieno quinoline and phthalic acid. More oxygen-containing compounds in treated wastewater, in comparison with raw wastewater, point to the partial degradation of parent compounds into more stable compounds by ring cleavage, oxidation and hydroxylation of aromatic ring structures. Since reactive radicals produced in this process are non-selective, a wide range of intermediates is reasonable and further oxidation of intermediates need relatively longer reaction times.

Conclusions

The synthesized Mn, Mo, La/TiO₂/AC nanocomposite showed high nano-photocatalytic activity in dye degradation. The influence of various operating conditions like pH, nanocomposite dosage, and dye concentration on dye degradation was evaluated. The results show the maximum removal efficiency of 91 % at initial dye concentration of 20 mg L⁻¹, pH of 3, and catalyst dosage of 2 g L⁻¹.

Also, high COD removal efficiency (84 %) in the treatment of textile wastewater at optimum operating conditions (pH = 3, catalyst dosage = 2 g L⁻¹, reaction time = 300 min), show the photocatalytic ability of the synthesized nanocomposite. Further research is required in order to reduce the nanocomposite consumption for field applications in future.

ACKNOWLEDGEMENTS

This paper is obtained from the thesis of Samaneh Mirali, which was supported financially by Ahvaz Jundishapur University of Medical Sciences (Grant no: ETRC 9322).

Table 5 – Main constituents of raw textile wastewater

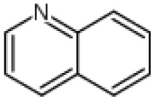
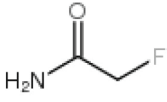
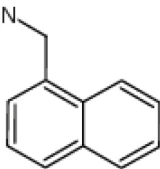
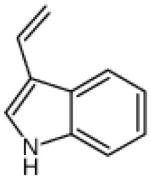
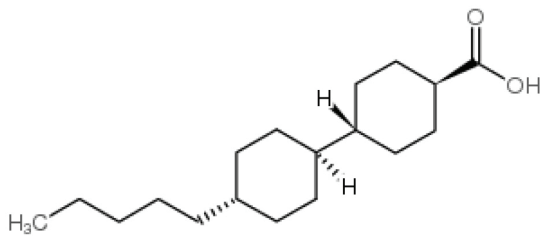
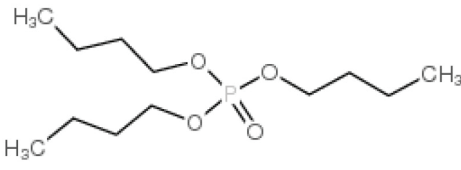
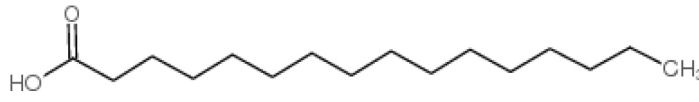
Substance	Structural formula	Chemical formula
Quinoline		C_9H_7N
Fluoroacetamide		C_2H_4FNO
Dimethylquinoline		$C_{11}H_{11}N$
Methylquinoline		$C_{10}H_9N$
Linoleic acid		$C_{18}H_{32}O_2$
Tri-butyl phosphate		$C_{12}H_{27}O_4P$
Palmitic acid		$C_{16}H_{32}O_2$

Table 6 – COD and TOC removal of raw textile wastewater using Mn, Mo, La/TiO₂/AC nano-photocatalytic degradation

Parameter	Raw wastewater	COD (mg L ⁻¹)						
		30 min	60 min	120 min	180 min	240 min	300 min	360 min
Total COD (mg L ⁻¹)	4700	4120	3652	2076	1438	1076	830	740
TOC (mg L ⁻¹)	3580	3190	2589	1328	1095	892	730	655

Table 7 – Main organic compounds identified in treated textile wastewater

Substance	Structural formula	Chemical formula
Acetamide		C_2H_5NO
Dimethyl propane		C_5H_{12}
Isoindole		C_8H_7N
Bromoform		$CHBr_3$
Methoxy phenyl benzoic acid		$C_{14}H_{12}O_3$
Cycloheptatriene		C_7H_8
Benzaldehyde		C_7H_6O
Benzoxazine		$C_8H_7NO_2$
Benzothieno quinoline		$C_{15}H_9NS$
Succinic acid		$C_4H_6O_4$
Phthalic acid		$C_8H_6O_4$

References

- Akar, S. T., Akar, T., Çabuk, A., Decolorization of a textile dye, reactive red 198 (RR198), by *Aspergillus parasiticus* fungal biosorbent, *Brazilian J. Chem. Eng.* **26** (2009) 399. doi: <https://doi.org/10.1590/S0104-66322009000200018>
- Jorfi, S., Barzegar, G., Ahmadi, M., Darvishi Cheshmeh Soltani, R., Jafarzadeh Haghighifard, N., Takdastan, A., Saeedi, R., Abtahi, M., Enhanced coagulation-photocatalytic treatment of Acid red 73 dye and real textile wastewater using UVA/synthesized MgO nanoparticles, *J. Environ. Manage.* **177** (2016)111. doi: <https://doi.org/10.1016/j.jenvman.2016.04.005>
- Wu, C. H., Effects of operational parameters on the decolorization of C.I. Reactive Red 198 in UV/TiO₂ based systems, *Dye. Pigment.* **77** (2008) 31. doi: <https://doi.org/10.1016/j.dyepig.2007.03.003>
- Ahmadimoghaddam, M., Mesdaghinia, A., Naddafi, K., Nasser, S., Mahvi, A. H., Vaezi, F., Nabizadeh, R., Degradation of 2,4-dinitrophenol by photo fenton process, *Asian J. Chem.* **22** (2010) 1009.
- Esmaeli, R., Hassani, A. H., Eslami, A., Ahmadi Moghadam, M., Safari, A., Di-(2-ethylhexyl) phthalate oxidative degradation by fenton process in synthetic and real petrochemical wastewater, *Iran. J. Environ. Health. Sci. Eng.* **8** (2011) 201.
- Ahmadi, M., Amiri, H., Martínez, S. S., Treatment of phenol-formaldehyde resin manufacturing wastewater by the electrocoagulation process, *Desalin. Water. Treat.* **39** (2012) 176. doi: <https://doi.org/10.1080/19443994.2012.669172>
- Anandan, S., Ikuma, Y., Murugesan, V., Highly active rare earthmetal La-doped photocatalysts: Fabrication, characterization, and their photocatalytic activity, *Int. J. Photoenergy* (2012) Article ID 921412. doi: <https://doi.org/10.1155/2012/921412>
- Hua, C., Dong, X., Wang, X., Xue, M., Zhang, X., Ma, H., Enhanced photocatalytic activity of W-doped and W-La-codoped TiO₂ nanomaterials under simulated sunlight, *J. Nanomater.* (2014) Article ID 943796. doi: <https://doi.org/10.1155/2014/943796>
- Reszczyńska, J., Grzyb, T., Sobczak, J. W., Lisowski, W., Gazda, M., Ohtani, B., Zaleska, A., Lanthanide co-doped TiO₂: The effect of metal type and amount on surface properties and photocatalytic activity, *Appl. Surf. Sci.* **307** (2014) 333. doi: <https://doi.org/10.1016/j.apsusc.2014.03.199>
- Devi, L. G., Kumar, S. G., Murthy, B. N., Kottam, N., Influence of Mn²⁺ and Mo⁶⁺ dopants on the phase transformations of TiO₂ lattice and its photocatalytic activity under solar illumination, *Catal. Commun.* **10** (2009) 794. doi: <https://doi.org/10.1016/j.catcom.2008.11.041>
- Wang, P., Yap, P., Lim, T., Applied Catalysis A: General C–N–S tridoped TiO₂ for photocatalytic degradation of tetracycline under visible-light irradiation, *Applied Catal. A, Gen.* **399** (2011) 252. doi: <https://doi.org/10.1016/j.apcata.2011.04.008>
- Zhou, M., Yu, J., Preparation and enhanced daylight-induced photocatalytic activity of C,N,S-tridoped titanium dioxide powders, *J. Hazard. Mater.* **152** (2008) 1229. doi: <https://doi.org/10.1016/j.jhazmat.2007.07.113>
- Jiang, H., Yan, P., Wang, Q., Zang, S., Li, J., Wang, Q., High-performance Yb, N, P-tridoped anatase-TiO₂ nano-photocatalyst with visible light response by sol-solvo-thermal method, *Chem. Eng. J.* **215-216** (2013) 348. doi: <https://doi.org/10.1016/j.cej.2012.10.082>

14. Shi, Z., Zhang, X., Yao, S., Synthesis and photocatalytic properties of lanthanum doped anatase TiO₂ coated Fe₃O₄ composites, *Rare Met.* **30** (2011) 252.
doi: <https://doi.org/10.1007/s12598-011-0377-3>
15. Ahmadi, M., Rahmani, K., Rahmani, A., Rahmani, H., Removal of benzotriazole by Photo-Fenton like process using nano zero-valent iron: response surface methodology with a Box-Behnken design, *Polish J. Chem. Technol.* **19** (2017)104.
doi: <https://doi.org/10.1515/pjct-2017-0015>
16. Ahmadi, M., Kakavandi, B., Jorfi, S., Azizi, M., Oxidative degradation of aniline and benzotriazole over PAC@Fe^{III}e₂mO₄: A recyclable catalyst in a heterogeneous photo-Fenton-like system, *J. Photochem. Photobiol. A Chem.* **336** (2017) 42.
doi: <https://doi.org/10.1016/j.jphotochem.2016.12.014>
17. Li, D., Xing, Z., Yu, X., Cheng, X., One-step hydrothermal synthesis of C-N-S-tridoped TiO₂ based nanosheets photo-electrode for enhanced photoelectrocatalytic performance and mechanism, *Electrochim. Acta.* **170** (2015)182.
doi: <https://doi.org/10.1016/j.electacta.2015.04.148>
18. Wang, W., Lu, C., Ni, Y., Su, M., Huang, W., Xu, Z., Preparation and characterization of visible-light-driven N-F-Ta tri-doped TiO₂ photocatalysts, *Appl. Surf. Sci.* **258** (2012)8696.
doi: <https://doi.org/10.1016/j.apsusc.2012.05.077>
19. Kim, H., Zhou, D., Wang, R., Jiao, Q., Yang, Z., Song, Z., Yu, X., Qiu, J., Effect of Mn 2⁺ ions on the enhancement red upconversion emission of Mn²⁺/Er³⁺/Yb³⁺ tri-doped in transparent glass-ceramics, *Opt. Laser Technol.* **64** (2014) 264.
doi: <https://doi.org/10.1016/j.optlastec.2014.05.002>
20. Lin, M. Z., Chen, H., Chen, W. F., Nakaruk, A., Koshy, P., Sorrell, C. C., Effect of single-cation doping and codoping with Mn and Fe on the photocatalytic performance of TiO₂ thin films, *Int. J. Hydrogen Energy* **39** (2014) 21500.
doi: <https://doi.org/10.1016/j.ijhydene.2014.02.013>
21. Ziyilan-Yavas, A., Mizukoshi, Y., Maeda, Y., Ince, N. H., Supporting of pristine TiO₂ with noble metals to enhance the oxidation and mineralization of paracetamol by sonolysis and sonophotolysis, *Appl. Catal. B Environ.* **7** (2015) 172.
22. Mamba, G., Mbianda, X. Y., Mishra, A. K., Photocatalytic degradation of the diazo dye naphthol blue black in water using MWCNT/Gd,N,S-TiO₂ nanocomposites under simulated solar light, *J. Environ. Sci.* **33** (2015) 219.
doi: <https://doi.org/10.1016/j.jes.2014.06.052>
23. Ellsami, L., Lachheb, H., Houas, A., Synthesis, characterization and photocatalytic activity of Li, Cd, and La doped TiO₂, *Mater. Sci. Semicond. Process* **36** (2015) 103.
doi: <https://doi.org/10.1016/j.mssp.2015.03.032>
24. Ma, L., Jia, I., Guo, X., Xiang, L., Current status and perspective of rare earth catalytic materials and catalysis, *Chinese J. Catal.* **35** (2014) 108.
doi: [https://doi.org/10.1016/S1872-2067\(12\)60720-7](https://doi.org/10.1016/S1872-2067(12)60720-7)
25. Jiang, H., Wang, Q., Zang, S., Li, J., Wang, Q., Enhanced photoactivity of Sm, N, P-tridoped anatase-TiO₂ nano-photocatalyst for 4-chlorophenol degradation under sunlight irradiation, *J. Hazard. Mater.* **261** (2013) 44.
doi: <https://doi.org/10.1016/j.jhazmat.2013.07.016>
26. Li, F., Yin, X., Yao, M. M., Li, J., Investigation on F-B-S tri-doped nano-TiO₂ films for the photocatalytic degradation of organic dyes, *J. Nanoparticle Res.* **13** (2011) 4839.
doi: <https://doi.org/10.1007/s11051-011-0461-5>
27. Li, Y., Zhou, X., Chen, W., Li, L., Zen, M., Qin, S., Sun, S., Photodecolorization of Rhodamine B on tungsten-doped TiO₂/activated carbon under visible-light irradiation, *J. Hazard. Mater.* **227–228** (2012) 25.
doi: <https://doi.org/10.1016/j.jhazmat.2012.04.071>
28. Umar, K., Haque, M. M., Muneer, M., Harada, T., Matsu-mura, M., Mo, Mn and La doped TiO₂: Synthesis, characterization and photocatalytic activity for the decolorization of three different chromophoric dyes, *J. Alloys Compd.* **578** (2013) 431.
doi: <https://doi.org/10.1016/j.jallcom.2013.06.083>
29. Chong, M. N., Jin, B., Chow, C. W. K., Saint, C., Recent developments in photocatalytic water treatment technology: A review, *Water Res.* **44** (2010) 2997.
doi: <https://doi.org/10.1016/j.watres.2010.02.039>
30. Quan, F., Hu, Y., Zhang, X., Wei, C., Simple preparation of Mn-N-codoped TiO₂ photocatalyst and the enhanced photocatalytic activity under visible light irradiation, *Appl. Surf. Sci.* **320** (2014) 120.
doi: <https://doi.org/10.1016/j.apsusc.2014.09.089>
31. Khairy, M., Zakaria, W., Effect of metal-doping of TiO₂ nanoparticles on their photocatalytic activities toward removal of organic dyes, *Egypt. J. Pet.* **3** (2014) 419.
32. Samet, L., Nasseur, J. Ben, Chtourou, R., March, K., Stephan, O., Heat treatment effect on the physical properties of cobalt doped TiO₂ sol – gel materials, *Mater. Charact.* **85** (2013) 1.
doi: <https://doi.org/10.1016/j.matchar.2013.08.007>
33. Bagheri, S., Ramimoghadam, D., Yousefi, A. T., Bee, S., Hamid, A., Synthesis, characterization and electrocatalytic activity of silver doped-titanium dioxide nanoparticles, *Int. J. Electrochem. Sci.* **10** (2015) 3088.
34. Berec, V., Characterization of La doped TiO₂ nanopowders by Raman spectroscopy, *Proc. Tenth Annu. Conf. Mater. Res. Soc. Serbia* **115** (2009) 771.
35. Duan, Y., Fu, N., Zhang, Q., Fang, Y., Zhou, X., Lin, Y., Influence of Sn source on the performance of dye-sensitized solar cells based on Sn-doped TiO₂ photoanodes: A strategy for choosing an appropriate doping source, *Electrochim. Acta.* **107** (2013) 473.
doi: <https://doi.org/10.1016/j.electacta.2013.06.085>
36. Cheng, X., Yu, X., Xing, Z., One-step synthesis of visible active CNS-tridoped TiO₂ photocatalyst from biomolecule cystine, *Appl. Surf. Sci.* **258** (2012) 7644.
doi: <https://doi.org/10.1016/j.apsusc.2012.04.111>
37. Akbarzadeh, R., Javadpour, S., W/Mo-doped TiO₂ for photocatalytic degradation of methylene blue, *Int. J. Eng. Sci. Innov. Technol.* **3** (2014) 621.
38. Liu, H., Lu, Z., Yue, L., Liu, J., Gan, Z., Shu, C., Zhang, T., Shi, J., Xiong, R., (Mo + N) codoped TiO₂ for enhanced visible-light photoactivity, *Appl. Surf. Sci.* **257** (2011) 9355.
doi: <https://doi.org/10.1016/j.apsusc.2011.05.085>
39. Li, Y., Chen, J., Liu, J., Ma, M., Chen, W., Li, L., Activated carbon supported TiO₂ photocatalysis doped with Fe ions for continuous treatment of dye wastewater in a dynamic reactor, *J. Environ. Sci.* **22** (2010)1290.
doi: [https://doi.org/10.1016/S1001-0742\(09\)60252-7](https://doi.org/10.1016/S1001-0742(09)60252-7)
40. Chen, M. L., Lim, C. S., Oh, W. C., Preparation with different mixing ratios of anatase to activated carbon and their photocatalytic performance, *J. Ceram. Process. Res.* **8** (2007)119.
41. Liu, Y., Yang, S., Hong, J., Sun, C., Low-temperature preparation and microwave photocatalytic activity study of TiO₂-mounted activated carbon, *J. Hazard. Mater.* **142** (2007) 208.
doi: <https://doi.org/10.1016/j.jhazmat.2006.08.020>

42. Malik, A., Hameed, S., Siddiqui, M. J., Haque, M. M., Muneer, M., Influence of Ce doping on the electrical and optical properties of TiO₂ and its photocatalytic activity for the degradation of Remazol Brilliant Blue R, *Environ. Sci. Technol.* **41** (2007) 4410.
43. Devi, L. G., Murthy, B. N., Characterization of Mo doped TiO₂ and its enhanced photo catalytic activity under visible light, *Catal. Letters* **125** (2008) 320.
doi: <https://doi.org/10.1007/s10562-008-9568-4>
44. Fan, T., Chen, C., Tang, Z., Ni, Y., Lu, C., Materials science in semiconductor processing synthesis and characterization of g-C₃N₄/BiFeO₃ composites with an enhanced visible light photocatalytic activity, *Mater. Sci. Semicond. Process* **40** (2015) 530.
doi: <https://doi.org/10.1016/j.mssp.2015.06.054>
45. Anil Kumar Reddy, P., Photocatalytic degradation of Isoproturon pesticide on C, N and S doped TiO₂, *J. Water Resour. Prot.* **2** (2010) 235.
doi: <https://doi.org/10.4236/jwarp.2010.23027>
46. Lu, N., Lu, Y., Liu, F., Zhao, K., Yuan, X., Zhao, Y., Li, Y., Qin, H., Zhu., H3PW12O₄₀/TiO₂ catalyst-induced photo-degradation of bisphenol A (BPA): Kinetics, toxicity and degradation pathways, *J. Chemosphere* **91** (2013) 1266.
doi: <https://doi.org/10.1016/j.chemosphere.2013.02.023>
47. Hamadani, M., Karimzadeh, S., Jabbari, V., Villagrán, D., Synthesis of cysteine, cobalt and copper-doped TiO₂ nanophotocatalysts with excellent visible-light-induced photocatalytic activity, *Mater. Sci. Semicond. Process* **41** (2016) 168.
doi: <https://doi.org/10.1016/j.mssp.2015.06.085>
48. Saggiaro, E. M., Oliveira, A. S., Pavesi, T., Maia, C.G., Ferreira, L. F. V., Moreira, J. C., Use of titanium dioxide photocatalysis on the remediation of model textile waste-waters containing azo dyes, *Molecules* **16** (2011) 10370.
doi: <https://doi.org/10.3390/molecules161210370>
49. Jorfi, S., Darvishi Cheshmeh Soltani, R., Ahmadi, M., Khatayee, A., Safari, M., Sono-assisted adsorption of a textile dye on milk vetch-derived charcoal supported by silica nanopowder, *J. Environ. Manage.* **187** (2017) 111.
doi: <https://doi.org/10.1016/j.jenvman.2016.11.042>